Article | Received 30 October 2024; Accepted 10 December 2024; Published 17 December 2024
https://doi.org/10.55092/am20240015

Quality prediction of semi-solid die casting of aluminum alloy in terms of machine learning

Zhiyuan Wang[1], Xiaogang Hu[2,*], Gan Li[1], Zhen Xu[1], Hongxing Lu[1], Qiang Zhu[1,*]

[1] Department of Mechanical and Energy Engineering, Southern University of Science and Technology, Shenzhen 518055, China
[2] School of Advanced Manufacturing, Sun Yat-Sen University, Shenzhen 518107, China

* Correspondence authors; E-mails: huxg6@mail.sysu.edu.cn (X. H.); zhuq@sustech.edu.cn (Q. Z.).

Abstract: Semi-solid die casting of aluminum alloy has been successfully employed to manufacture high-performance components with precise net shapes. However, the quality of these components is highly susceptible to variations in both environmental conditions and process parameters, leading to a narrow process window that restricts its widespread application in engineering. In this study, a machine learning (ML) model has been developed to identify defective products through the detection of injection pressure, thereby providing a foundation for monitoring and further optimizing the manufacturing process. Among various ML algorithms, the Multilayer Perceptron (MLP) is the most effective for overall quality prediction. Additionally, the mechanism for identifying defect types based on pressure curves has been revealed: the filling pressure at the gate entrance has been found to exhibit a strong correlation with the internal quality of the casting, while the V-P transition point has been identified as a reliable indicator of the external quality.

Keywords: semi-solid processing; die casting; machine learning; quality classification; injection pressure

1. Introduction

Semi-solid processing (SSP), in which the liquid-solid mixed slurry is used as the feedstock, is a promising forming technology for fabricating high-performance components with low loss and a short process [1–3]. Compared to traditional die casting with full liquid melt, semi-solid die casting applies a higher viscous slurry and fills the die cavity with laminar flow, thus avoiding entrapment defects and enhancing the mechanical properties [4,5]. SSP has been successfully applied in 5G communication cavities, automotive inverter main boxes, battery brackets, and other components [6].

Copyright©2024 by the authors. Published by ELSP. This work is licensed under Creative Commons Attribution 4.0 International License, which permits unrestricted use, distribution, and reproduction in any medium provided the original work is properly cited.

Despite the above-mentioned advantages of SSP, the final quality of the semi-solid die casting is more difficult to control due to the narrow process window. Process parameters such as filling pressure and injection velocity, which are significantly affected by slurry temperature, play crucial roles in determining the final quality of the manufactured components [7–11]. The quality of castings is closely related to the defect levels. In semi-solid die castings, defects are mainly classified into two categories: external defects and internal defects. External defects primarily refer to non-filling because of insufficient melt fluidity, while internal defects primarily refer to gas pores entrapped during mold filling and shrinkage cavities resulting from inadequate feeding during solidification [12,13]. Therefore, there may be a way to predict the possibility of defects in the manufactured components by studying filling pressure [14,15].

In previous work on die-casting, quality prediction has been performed mainly based on processing parameters or detecting environmental parameters. Winkler [16] emphasized the impact of real-time parameters like piston speed and temperature on porosity rate. Soban [17] explored the relationship between acceleration positions, velocity, and air entrapment profiles to optimize process parameters. Kittur [18] utilized a neural network algorithm to relate process parameters to quality parameters like surface roughness and porosity. Gim [19] utilized transfer learning to optimize artificial neural networks and successfully predicted the surface quality of injection-molded parts using five essential process parameters. Kim [20] developed defect rate diagnostic systems based on velocity and pressure time series, favoring tree-based regression algorithms. Lin [21] and Weiderer [22] employed data filtering and transformation techniques to improve efficiency and uncover quality-related issues. Chanbeom [23] used feature selection and neural networks to identify optimal manufacturing parameters. Deng [24] introduced time interval importance curves for classification, improving computational efficiency in analyzing time series data. All of these works were successful in building up the relationship between process parameters and the cast components, leading to the improvement of component quality and production efficiency. Semi-solid processing (SSP) uses semi-solid slurry instead of liquid metals as in conventional casting processes, and rheological characteristics play a crucial role in process control and component quality. Therefore, the conventional casting quality prediction approaches are difficult to adapt directly to the SSP process. In this work, a prediction model for the quality of semi-solid die-castings will be developed to predict the quality of SSP-processed components in terms of the injection pressure.

2. Methods

Figure 1 shows the basic flow of the die-casting quality prediction module and the evaluation of important processing intervals. First, the pressure and displacement data from the die-casting plunger sensors are processed, and then features are extracted from the processed data. The model building was based on both the raw data and the processed characteristics. Furthermore, both sets will be compared with each other. It is clear that two quality prediction systems have been developed: one for the diagnosis of internal defects and another for the

diagnosis of external defects. A validation set is set up, with data sourced from the pressure casting of 319s aluminum alloy. The best results will be based on the comparison of the scores of the models training.

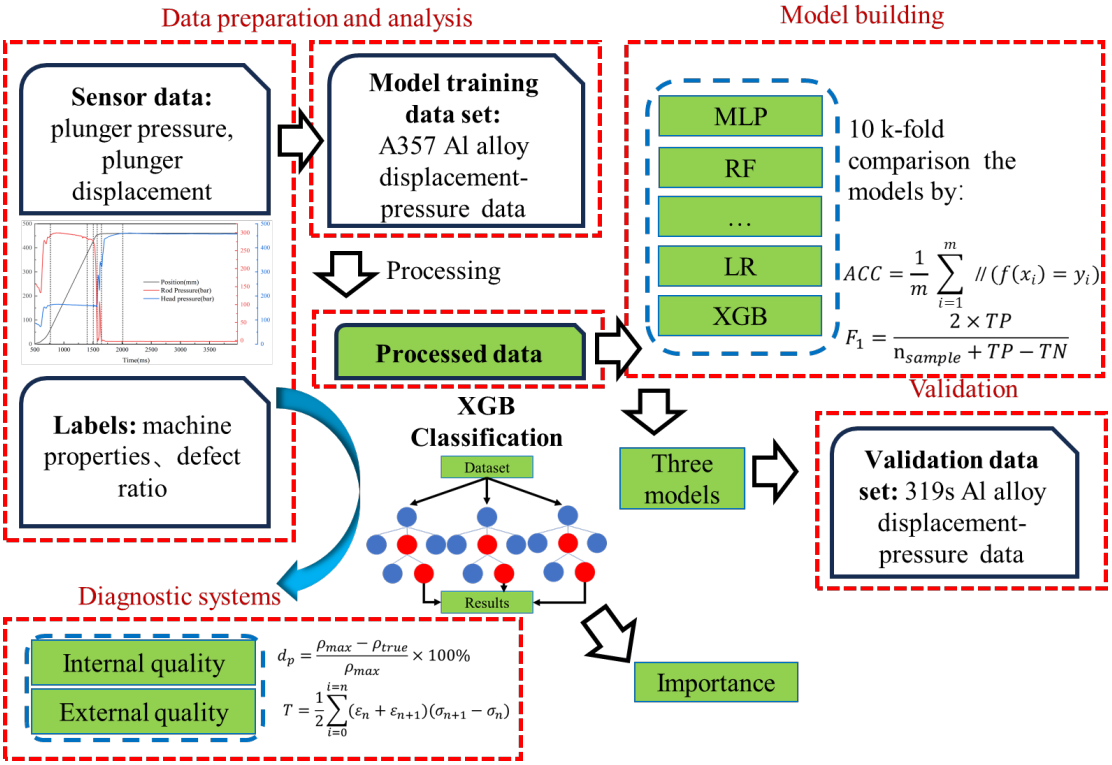

Figure 1. Basic flow of the die casting quality prediction module and evaluation of important processing intervals.

2.1. Slurry preparation and die casting

Table 1 shows the chemical composition of commercial aluminum alloys A357 and 319s used in this study. There is a difference in the contents of Mg, Si, and Cu between these two alloys. Figure 2 shows the flow of the experiments. About 55 kg of aluminum alloy materials were melted in the furnace and degassed at 770 °C for 30 min. A crucible was used to take approximately 1.65 kg of melt from the furnace and then cooled down to specified temperatures. The semi-solid slurry was prepared using the swirled enthalpy equilibration device (SEED) [25]. Four different groups of parameters of the rotation time and the pouring temperatures in SEED processes are given in Table 2.

The slurry was die-cast into tensile specimens by a die-casting machine (FRECH K380–40) with the max plunger velocity of 0.5 m/s (constant). The maximum pressure of the plunger was set to 460 bar. The preheating temperature of the mold was 260 °C. The experiment samples were die-casted using the tooling shown in Figure 3a, and four rods were cut off and then machined into tensile testing specimens, as shown in Figure 3b.

Table 1. Chemical composition of the experimental aluminum alloys (wt %).

Alloy	Al	Mg	Cu	Si
A357	Bal.	0.61	<0.01	7.30
319s	Bal.	0.36	3.05	6.10

Table 2. Rotation time and pouring temperature in semi-solid slurry preparation.

Alloys	Groups	A	B	C	D
A357	Pouring temperature (°C)	615	630	630	675
	Rotation time (s)	90	90	150	150
319s	Pouring temperature (°C)	615	635	635	675
	Rotation time (s)	90	90	150	150

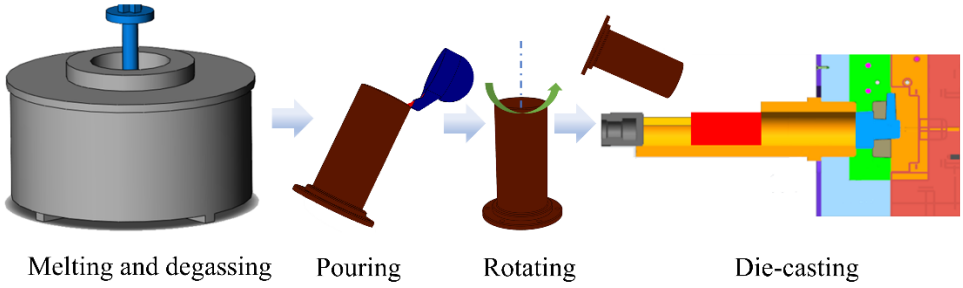

Figure 2. The experiment flow of slurry making and die casting in this research.

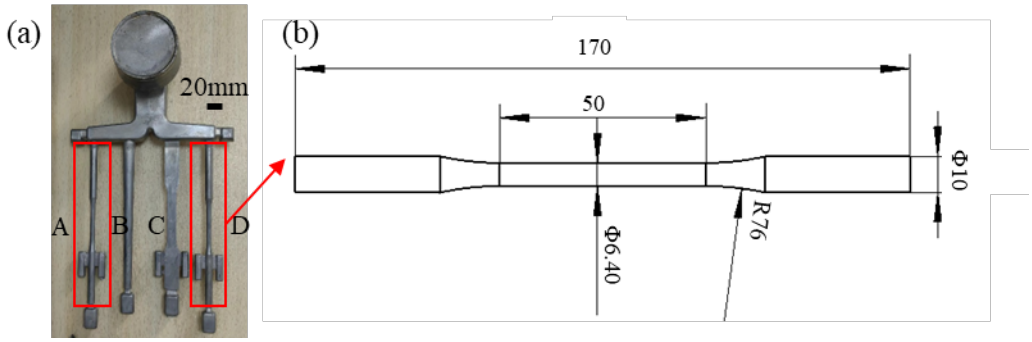

Figure 3. (a) Die casting component and **(b)** sample size for tensile testing.

2.2. Record of plunger pressures

Three sensors were installed at the die-casting machine's plunger, which recorded the pressure at the head of the plunger, the pressure at the rod part of the plunger, and the displacement of the plunger, respectively. Data were collected at intervals of 2 ms, and each sensor recorded 2000 data during die-casting. Figure 4 shows the pressure and plunger displacement changes obtained from the three sensors with processing time.

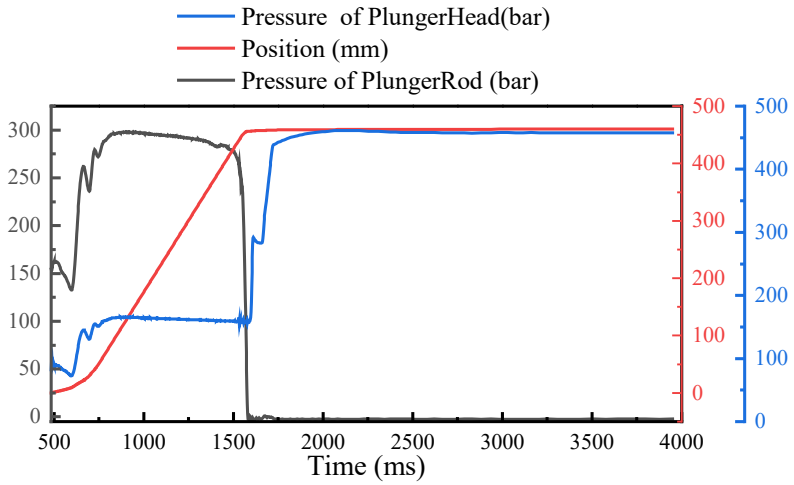

Figure 4. Pressures obtained from the sensors of the plunger head and rod, and displacement with time.

2.3. Tensile tests and defect identification

A INSTRON 3382 tensile testing machine was employed to perform the tensile tests. The movement speed of the testing head was 0.5 mm/s until the strain of 0.6 and 5 mm/s after removing the extensometer. The static toughness of the testing sample $T(N)$ was determined as follows:

$$T(N) = \frac{1}{2}\sum_{0}^{n-1}((\sigma_N + \sigma_{N+1}) \cdot (\varepsilon_N - \varepsilon_{N+1})) \quad (1)$$

where n is the amount of data set, tensile strain $\varepsilon = [\varepsilon_1, \varepsilon_2, \cdots, \varepsilon_n]$ and tensile stress $\sigma = [\sigma_1, \sigma_2, \cdots, \sigma_n]$. The defect level was determined by the liquid static weighing method. Each value was the average data of three measurements. The mass densities were measured by a density measurement device based on Archimedes principle. The relative defect ratio d was calculated by:

$$d = \frac{d_m - d_a}{d_m} \times 100\% \quad (2)$$

where d_a is the density of the testing sample and d_m is the standard density of this alloy.

2.4. Casting quality definition

There are two definitions for casting quality, *i.e.*, internal defects and externally visible defects. The evaluation indicators for internal quality were the defect rate of castings and static toughness, but it was challenging to define thresholds for the two quality categories. As a highly popular clustering algorithm for unsupervised learning, the K-means clustering was employed to divide these two data types into several clusters, as shown in Figure 5a. Finally, clusters with low defect rates and excellent mechanical performance were selected as class I1, while the rest will be categorized as I0. A t-distribution is used for the result, using a 95% confidence interval. In addition, the proportion of data for different categories

is also taken into consideration. Figure 5b shows the relevant details: samples labeled as E0 exhibit a non-fill phenomenon, while those labeled as E1 do not. At the bottom of Figure 5, categories with both positive and negative proportions under each standard are displayed, and this proportion is relatively reasonable.

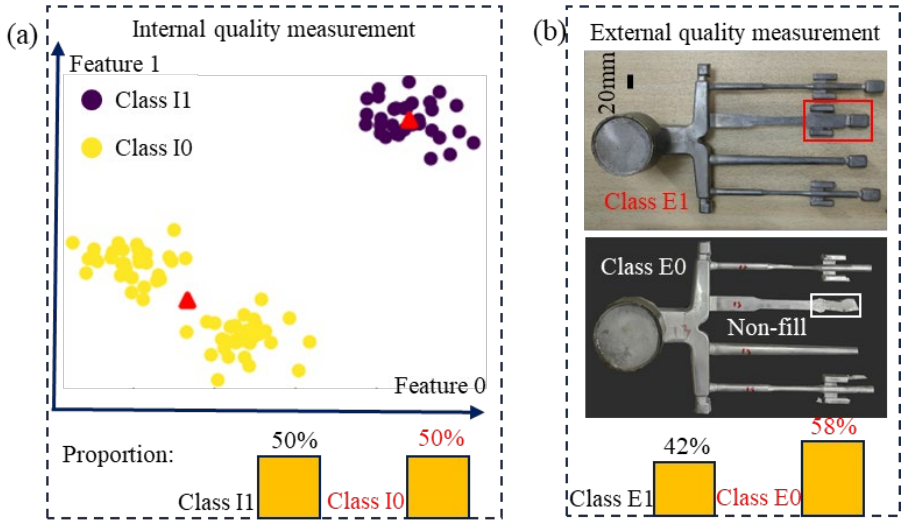

Figure 5. Two quality classifications: **(a)** internal quality measurement (K-means clusters), **(b)** external defects, which are mainly the non-filled castings defined as class E0, while fully cast components defined as class E1.

2.5. Machine learning models and evaluation

Machine learning algorithms such as support vector machine (SVM) [26,27], the multilayer perceptron (MLP) [28], random forest (RF) [29], gradient boosting classifier (GBC) [30], extreme gradient boosting (XGB) [31], decision tree (DT) [32], logic regression (LR) [33] and Light Gradient Boosting Machine (LGB) [34] are employed in this research. These models are commonly used for quality prediction of manufactured components [35].

The selected features data were normalized before training the machine learning system. The average score was determined using ten k-fold cross-validations, and the best strategy was found by comparing the experimental results. The validation assessment of the models was achieved using the accuracy (ACC), the areas under the ROC curve (AUC), the F1 score, the Recall score, and the Precision score. ACC and F1 scores [36–38] are expressed as follows:

$$ACC = \frac{TP + TN}{TP + TN + FN + FP} \tag{3}$$

$$F1 = \frac{2 \cdot TP}{2TP + FN + FP} \tag{4}$$

$$Recall = \frac{TP}{TP + FP} \tag{5}$$

$$Precision = \frac{TP}{TP + FN} \tag{6}$$

Where TP is the abnormal castings that are classified correctly, TN is that the normal castings are identified correctly, FP represents that the class 1 castings are misclassified as class 0 ones, and FN represents the class 0 castings are mistakenly classified as class 1 ones.

3. Results and discussion

3.1. Recorded data analysis

The pressure data, defined as the injection pressure P_p, measured by the sensor installed in the plunger of the die casting machine, were employed to be the input data of the machine learning modelling, as they can reflect the resistance of the semi-solid slurry filled into the tooling. The injection pressure P_p can be expressed as:

$$P_p = P_{Head} - P_{Rod} \tag{7}$$

where P_{Head} is the pressure at the plunger head, P_{Rod} is the pressure at the plunger rod. Due to the difference in slurry weight among different dies, the offset displacement, *i.e.*, the abscissa of the die-casting curve, is corrected. The corrected abscissa formula is that:

$$D_c = D_p - (D_{max} - \frac{V}{S_p}) \tag{8}$$

where D_c is the corrected displacement coordinate, D_p is the displacement coordinate coming from the plunger position sensor, V is the volume of the casting, S_p is the area of the plunger, D_{max} is the maximum value of the displacement of the plunger. Figure 6 shows the changes in pressure and velocity following the alteration of the abscissa.

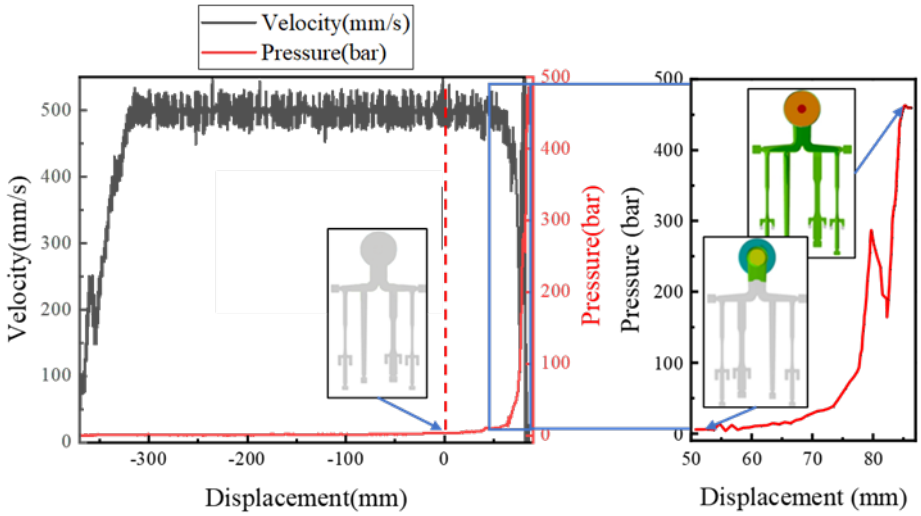

Figure 6. The pressure P_p and plunger speed *versus* the plunger displacement after the slurry contacts the slider.

During a semi-solid die-casting process, the slurry contacts the slider at the displacement of 0 mm, and then the plunger pushes the slurry to move at the set speed (0.5 m/s). At this time, the pressure mainly reflects the resistance of the plunger pushing the slurry to move in the pipeline. With the plunger moving continuously, pressure increases quickly as the slurry

is pushed into the gate. The velocity of the plunger is no longer stable, falling to less than 98% of the set value. When the plunger reaches the position of 86 mm, the pressure reaches the maximum, and the velocity closes to zero. At this time, the slurry almost fills the mold, and the plunger can hardly move. Thus, the plunger position of 50–86 mm is regarded as an essential interval of die casting. Figure **7** shows the evolution characteristics of both the raw recorded pressure data and the processing pressure data with displacement movement at this crucial stage. Figure **7**a shows the original injection data. Dividing this important interval into 36 equal parts, the average pressure for each part forms the curve shown in Figure **7**b.

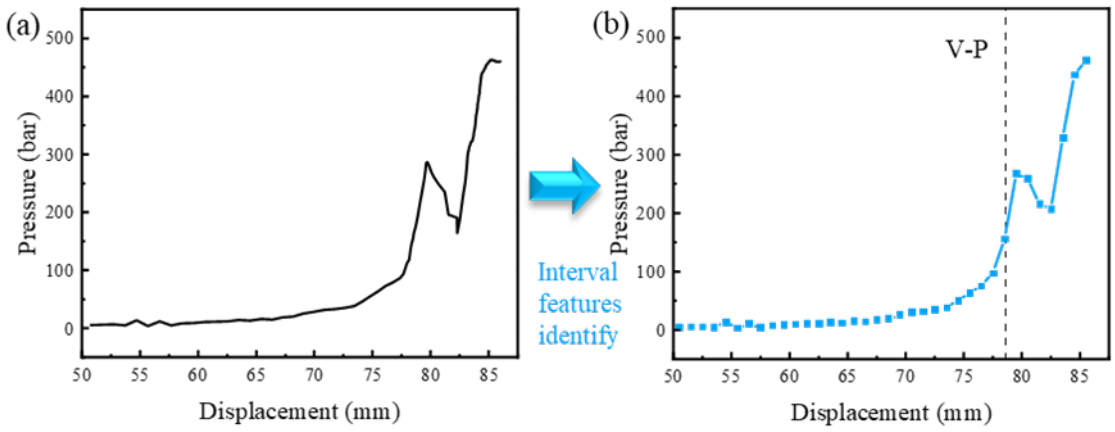

Figure 7. The pressure *versus* the corrected displacement D_c: **(a)** injection pressure P_p and **(b)** processing data within the interval.

In order to enhance the results, five characteristics were determined, *i.e.*, the pressure at the plunger displacement of 423 mm (the maximal displacement), an average pressure at the plunger position of 50–86 mm, points where pressurization is started, and points that the value of the rod pressure is 0. The maximum pressure reading from the head pressure sensor within 1.5 s is taken as the critical value. Any point thereafter where the pressure exceeds this value is considered as the moment when pressurization begins. In general, 41 features exist for data training. Compared to the raw data recorded by sensors, this dataset has reduced its scale from 6000 to 41. Table 3 shows the recorded characteristic data of the pressure curve and its related quality classification, which will be employed in the model training. To assess the efficiency of the data selection, the raw data from three sensors and the selected data were separately used as the features for training.

Table 3. The recorded characteristic data of the pressure curve and its related quality class.

Number	Interval 1 (bar)	Interval 2 (bar)	…	Interval 36 (bar)	Pressurization point (mm)	Internal quality	External quality
0	4.93	5.25	…	459.36	82.78	I1	E0
1	6.25	6.35	…	460.68	82.28	I1	E0
⋮	⋮	⋮		⋮	⋮	⋮	⋮
107	9.17	9.46	…	460.84	79.25	I0	E1

3.2. Model training results

The results of ten-fold cross-validation were compared, as shown in Figure 8. The training results used raw data on both internal and external defects without considering the data characteristics. The model SVM achieved the highest accuracy ACC score of 0.8429, with an AUC score of 0.8828 and an F1 score of 0.8677. The models LGB and RF achieved a recall score of 0.90, indicating good classification performance for positive samples, while MLP achieved only 0.7383, which did not meet the requirements for this study. For the selected characteristic data, however, the performance of the MLP achieved an ACC score of 0.9238, an F1 score of 0.9373, and an AUC score of 0.9525, the best model for quality prediction for both internal and external defects, as shown in Figure 8c,d, and significant higher ACC than using the raw data with increases of 9.6% in ACC score, 8% in F1 score, and 5.6% in AUC. Therefore, training with filtered data in this classification contributes to enhancing the model's generalization ability. The model MLP would be employed to be trained by the characteristic data and to predict the casting quality.

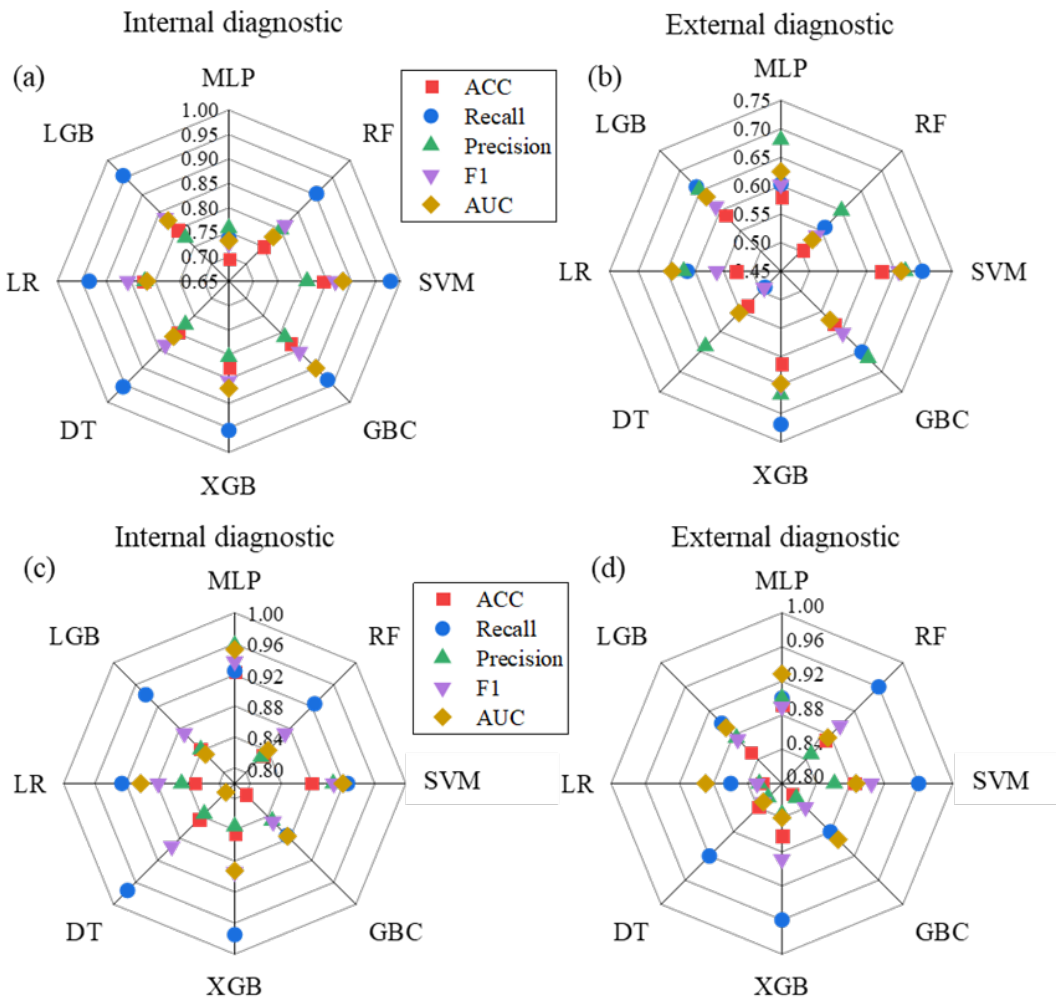

Figure 8. The results of predicted quality determined by all the models considered in this study for **(a)** raw data for internal, **(b)** raw data for external defects, **(c)** characterized data for internal, **(d)** characterized data for external defects.

The tenfold cross-validation results for training on raw data are presented in Figure 8b. Unfortunately, none of the models achieved a validation accuracy exceeding 0.7. Additionally, the performance in terms of AUC and F1 scores was also not good. Therefore, the raw pressure values alone as characteristic data were insufficient to meet the requirements of external defect classification. In addition to the characterized plunger pressure, characteristic data such as the pressurization point and the maximum plunger displacement were also considered in training the models. These characteristic data are also correlated with external defects (*i.e.*, quality). Figure 8d shows the training results after incorporating these characteristic data.

The classification model trained by the MLP model made the best scores of ACC and AUC and could predict the casting quality with a confidence of 0.89. However, it is worth noting that the F1 score of the MLP model is lower than the RF and SVM models. In terms of recall scores, the MLP model scored 6.3% lower than the other two models, while the precision score is 4.5% and 6.0% higher. This means that the MLP model predicts the correct sample better, and there are a few false positive cases, but it cannot find all of the positives. In practice, predicting negatives as positives is not permissible; the cost of missing positives is relatively smaller. Therefore, the MLP model is the best prediction strategy for this classification.

3.3. Application of the trained models for the 319s alloy castings

The trained MLP, XGB, and LGB models were applied to predict the quality of semi-solid die castings of the aluminum alloy 319s, which has higher contents of Cu and Si but lower content of Mg. The semi-solid die casting of this alloy had almost no external defects, so only internal defects were predicted and compared with experimental results. Generally, the models were used to produce predictive probabilities for both positive and negative instances. They were then translated into confidence levels for positive predictions in practical applications. Figure 9 shows the validation results of the three models on the 319s die-casting pressure dataset mentioned above. In this case, the probability of being predicted as positive issues (good quality) was taken as the Z-axis, while the X and Y coordinates represent mechanical properties and defect rates. Mechanical properties and defect rates are assessment metrics for internal quality, respectively. The yellow areas in the figures indicate regions classified as positive issues, while the blue planes (Z = 0.5) represent the boundaries between positive and negative predictions. The results indicate that XGB and MLP get the best validation ACC scores of 0.8517. XGB identifies all positive samples, while LGB misclassifies 57% of positives as negatives. Conversely, LGB can find all negatives, but XGB exhibits excessive sensitivity to positives. Therefore, it can be observed in Figure 9d that LGB has a lower F1 score than others. For the AUC score, XGB is above 0.9 and gets the best performance, which implies that different thresholds result in stronger classification capability. For the F1 score, The LGB model is lower than that of MLP and XGB. Therefore, compared to LGB and MLP, XGB demonstrates superior generalization ability, undoubtedly making it more suitable for serving as the final predictive model.

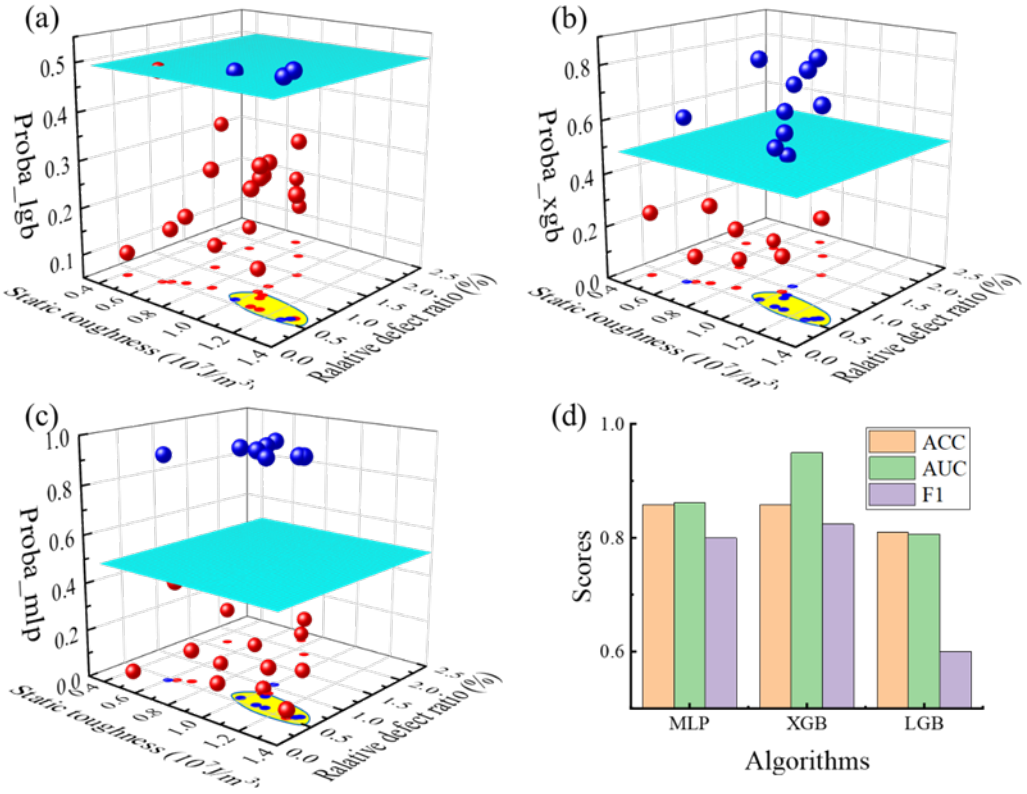

Figure 9. The prediction results of internal quality of the aluminum alloy 319s semi-solid die-castings by different models: **(a)** LGB, **(b)** XGB, **(c)** MLP, and **(d)** testing scores of validations of these models: ACC, AUC, F1.

3.4. Interval feature results

In order to understand the detailed relationship between casting quality and displacement of the plunger during die casting, the displacement between 50 and 86, which represents the start and end of filling the mold of semi-solid slurry, was divided into 36 intervals. Figure 10a presents four typical curves of pressure *versus* displacement, *i.e.*, without internal defects (internal 1) and without external defects (external 1), without internal defects (internal 1) and with external defects (external 0), with internal defects (internal 0) and without external defects (external 1) as well with internal defects (internal 0) and with external defects (external 0).

The injection pressure curves for different categories are compared in Figure 10b, along with the plunger position at the onset of pressurization. The orange boxed area in the picture represents a section after the slurry enters the gate. The pressure in this section can reflect the internal quality of the castings. At this point, the pressure mainly reflects the resistance during the cavity filling. The enlarged area in the picture shows pressure changes after entering the sprue. It is apparent that during the filling stage, poor internal quality correlates with high pressure. The greater the filling resistance, the more likely internal defects are to occur.

For external defects, the green-boxed region holds significant influence. It is worth noting that the nodes of velocity-pressure conversion also wield considerable external impact, which confirms the necessity of individually extracting this data. As depicted in the figure, castings without noticeable external defects exhibit nodes quite early. When entering

the area of the green box on the left, the pressure values of different external quality classes have already begun to diverge. At this point, the pressure curve corresponding to the castings with better surface quality significantly increases, indicating the beginning of pressurization. If the temperature of the semi-solid slurry is high, resulting in a more considerable volume shrinkage, it manifests as a greater distance of movement of the piston after pressurization. Higher temperature semi-solid slurry results in better surface quality due to its stronger filling capability. If the temperature of the slurry is low, the flow may cease prematurely. Once grain coalescence forms a network, it significantly increases the resistance to filling, reflecting a rapid rise in pressure. In other words, the pressure values in the figure swiftly rise from below 50 bar to 300 bar. Because the model can capture these key features and nodes during training, it can accurately assess the filling capacity of the slurry and provide a reasonable likelihood of defect occurrence.

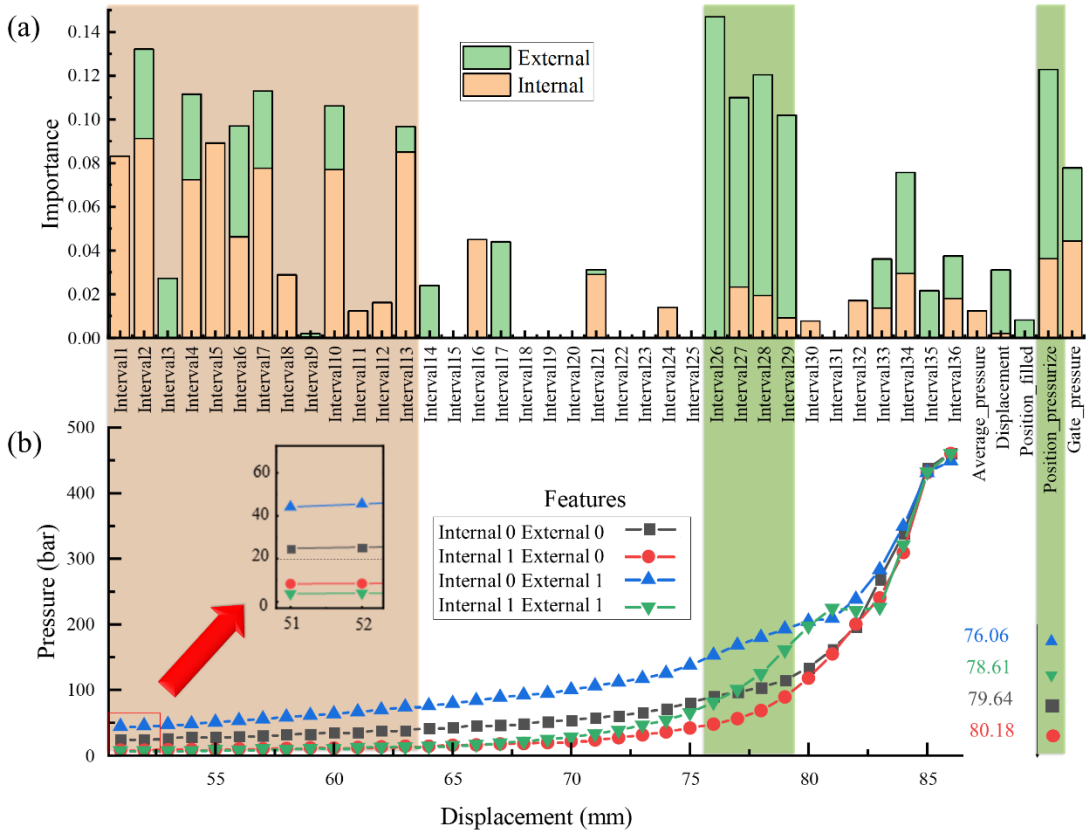

Figure 10. (a) The feature importance results are provided by the extreme gradient boosting (XGB), **(b)** corresponding die casting curves for four typical curves of pressure *versus* displacement.

4. Conclusion

The paper presents a quality prediction model for semi-solid die-cast components, leveraging displacement and plunger pressure as foundational parameters. The final verification results demonstrate that this prediction model can be applied to Al-Si alloys and SSP processes. In particular, some conclusions are summarized as follows:

(1) For data preparation, due to the introduction of data slicing and curve node extraction based on domain knowledge, important processing intervals corresponding to each casting can be accurately identified, which plays a crucial role in successfully identifying defective die castings. Training with selected data yields better results than with the raw data recorded by the three sensors. For accuracy (ACC) scores, internal diagnostic prediction improves by 9.6%, while external diagnostic prediction improves by 53%.

(2) These features were used for training and comparing eight machine learning algorithms. The best prediction effect obtained in the overall quality prediction is MLP, where the ten k-fold cross-validation accuracy score reaches 0.9238. In predicting 319s Al alloy quality, MLP and XGB models obtained equal results with additional conditions, and the ACC score is 0.8571. The generalizability of the model is proved, and it can be used to predict other alloy processing.

(3) The feature importance analysis indicates that, in the proposed gating-pressure coordinate system, the filling pressure upon entering the gate can be correlated with the internal quality of the casting, while the V-P transition point during die casting reflects the external quality of the casting. To obtain castings with fewer defects and better surface finish, it is necessary to reduce the filling pressure and provide sufficient movement distance to the plunger after the V-P transition. Therefore, in semi-solid die casting, attention needs to be paid to the filling pressure and the V-P transition point.

Supplementary data

The data supporting the findings of this study are available within the paper.

Acknowledgment

This work is financially supported by the National Natural Science Foundation of China (52474409), Shenzhen Science and Technology Innovation Commission (GJHZ20240218111359003), and the High level of special funds (G03034K003) from SUSTech.

Conflicts of interests

The authors declare no other competing interests.

Authors' contribution

Conceptualization, X.H. and Q.Z.; methodology, Z.W.; validation, G.L. and X.Z.; investigation, Z. W.; data curation, H.L.; writing—original draft preparation, Z.W.; writing—review and editing, X.H. and Q.Z.; supervision, X.H.; funding acquisition, Q.Z. All authors have read and agreed to the published version of the manuscript.

References

[1] Spencer DB, Mehrabian R, Flemings MC. Rheological behavior of Sn-15 pct Pb in the crystallization range. *Metall. Trans.* 1972, 3(7):1925–1932.

[2] Hu XG, Hu ZH, Qu WY, Li XW, Li Z, *et al.* A novel criterion for assessing the

processability of semi-solid alloys: The enthalpy sensitivity of liquid fraction. *Materialia* 2019, 8:100422.
[3] Qu W, Li D, Zhang F, Luo M, Hu X, *et al.* Multiphase modelling of the transient flow for Sn-15Pb and 357.0 alloys in semi-solid die casting process. *J. Mater. Process. Technol.* 2020, 278:116534.
[4] Atkinson H. Current status of semi-solid processing of metallic materials. In *Advances in Material Forming*, Paris, France, 2007, pp. 81–98.
[5] Kapranos P. Current state of semi-solid net-shape die casting. *Metals* 2019, 9(12):1301.
[6] Li G, Qu WY, Luo M, Cheng L, Guo C, *et al.* Semi-solid processing of aluminum and magnesium alloys: Status, opportunity, and challenge in China. *Trans. Nonferrous Met. Soc. China*. 2021, 31(11):3255–3280.
[7] Midson SP. Industrial applications for aluminum semi-solid castings. *Solid State Phenom.* 2015, 217–218:487–495.
[8] Laws KJ, Gun B, Ferry M. Effect of die-casting parameters on the production of high quality bulk metallic glass samples. *Mater. Sci. Eng. A* 2006, 425(1):114–120.
[9] Rai JK, Lajimi AM, Xirouchakis P. An intelligent system for predicting HPDC process variables in interactive environment. *J. Mater. Process. Technol.* 2008, 203(1):72–79.
[10] Xu C, Zhao J, Guo A, Li H, Dai G, *et al.* Effects of injection velocity on microstructure, porosity and mechanical properties of a rheo-diecast Al-Zn-Mg-Cu aluminum alloy. *J. Mater. Process. Technol.* 2017, 249:167–171.
[11] Zhang H, Li DQ, Qu WY, Zhang F, Luo M, *et al.* Effect of primary α-Al morphology in slurry on segregation. *Solid State Phenom.* 2019, 285:398–402.
[12] Hu XG, Zhu Q, Midson SP, Atkinson HV, Dong HB, *et al.* Blistering in semi-solid die casting of aluminium alloys and its avoidance. *Acta Mater.* 2017, 124:446–455.
[13] Hu XG, Zhu Q, Atkinson HV, Lu HX, Zhang F, *et al.* A time-dependent power law viscosity model and its application in modelling semi-solid die casting of 319s alloy. *Acta Mater.* 2017, 124:410–420.
[14] Ling Y, Zhou J, Nan H, Yin Y, Shen X. A shrinkage cavity prediction model for gravity castings based on pressure distribution: A casting steel case. *J. Manuf. Processes* 2017, 26:433–445.
[15] Leonardo P, Marco S, Giovanni L. Influence of the injection molding thermal boundary conditions on the filling flow of PET. *J. Manuf. Processes* 2022, 81:807–816.
[16] Winkler M, Kallien L, Feyertag T. Correlation between process parameters and quality characteristics in aluminum high pressure die casting. In *NADCA Die Casting Congress and Exposition*, Chicago, USA, 5–7 October 2015.
[17] Soban D, Thornhill D, Salunkhe S, Long A. Visual analytics as an enabler for manufacturing process decision-making. *Procedia CIRP* 2016, 56:209–214.
[18] Kittur JK, Manjunath Patel GC, Parappagoudar MB. Modeling of pressure die casting process: an artificial intelligence approach. *Int. J. Metalcast.* 2016, 10(1):70–87.
[19] Gim J, Yang H, Turng LS. Transfer learning of machine learning models for multi-objective process optimization of a transferred mold to ensure efficient and robust injection molding of high surface quality parts. *J. Manuf. Processes* 2023, 87:11–24.
[20] Kim JS, Kim J, Lee JY. Die-casting defect prediction and diagnosis system using process condition data. *Procedia Manuf.* 2020, 51:359–364.
[21] Lin CH, Hu GH, Ho CW, Hu CY, Kuo PC. Press casting quality detection and analysis based on machine learning. In *2021 International Symposium on Intelligent Signal Processing and Communication Systems (ISPACS)*, 16–19 November 2021, pp. 1–2.
[22] Weiderer P, Tomé AM, Lang EW. A NMF-based extraction of physically meaningful components from sensory data of metal casting processes. *J. Manuf. Syst.* 2020, 54:62–73.
[23] Bak C, Roy AG, Son H. Quality prediction for aluminum diecasting process based on shallow neural network and data feature selection technique. *CIRP J. Manuf. Sci.*

Technol. 2021, 33:327–338.
[24] Deng H, Runger G, Tuv E, Vladimir M. A time series forest for classification and feature extraction. *Inf. Sci.* 2013, 239:142–153.
[25] Luo M, Li D, Qu W, Hu X, Zhu Q, *et al.* Mold-slug interfacial heat transfer characteristics of different coating thicknesses: effects on slug temperature and microstructure in swirled enthalpy equilibration device process. *Materials* 2019, 12(11):1836.
[26] Burges CJC. A tutorial on support vector machines for pattern recognition. *Data Min. Knowl. Discovery* 1998, 2(2):121–167.
[27] Vapnik VN. An overview of statistical learning theory. *IEEE Trans. Neural Networks* 1999, 10(5):988–999.
[28] Rosenblatt F. Perceptron simulation experiments. *Proc. IRE* 1960, 48(3):301–309.
[29] Tin Kam H. The random subspace method for constructing decision forests. *IEEE Trans. Pattern Anal. Mach. Intell.* 1998, 20(8):832–844.
[30] Sigrist F. Gradient and Newton boosting for classification and regression. *Expert Syst. Appl.* 2021, 167:114080.
[31] Chen T, Guestrin C. XGBoost: A scalable tree boosting system. In *Proceedings of the 22nd ACM SIGKDD International Conference on Knowledge Discovery and Data Mining*, New York, USA, 2016, pp. 785–794.
[32] Quinlan JR. Simplifying decision trees. *Int. J. Man Mach. Stud.* 1987, 27(3):221–234.
[33] Boyd CR, Tolson MA, Copes WS. Evaluating trauma care: The TRISS method. *J. Trauma Acute Care* 1987, 27(4):370–378.
[34] Ke GL, Meng Q, Thomas F, Wang TF, Chen W, *et al.* LightGBM: A highly efficient gradient boosting decision tree. *Adv. Neural Inf. Process. Syst.* 2017, 30:3149–3157.
[35] Fahle S, Prinz C, Kuhlenkötter B. Systematic review on machine learning (ML) methods for manufacturing processes—Identifying artificial intelligence (AI) methods for field application. *Procedia CIRP* 2020, 93:413–418.
[36] Hanley JA, McNeil BJ. A method of comparing the areas under receiver operating characteristic curves derived from the same cases. *Radiology* 1983, 148(3):839–843.
[37] Hand DJ, Till RJ. A simple generalisation of the area under the ROC curve for multiple class classification problems. *Mach. Learn.* 2001, 45(2):171–186.
[38] Taha AA, Hanbury A. Metrics for evaluating 3D medical image segmentation: analysis, selection, and tool. *BMC Med. Imaging* 2015, 15(1):29.